Letter

Role of on-site Coulomb interactions in the half-metallic Weyl ferromagnet candidate thin-film Co_2FeSi

Kazuki Sumida,[1,*] Yuichi Fujita,[2] Weinan Zhou,[2] Keisuke Masuda,[2] Ikuto Kawasaki,[1] Shin-ichi Fujimori,[1] Akio Kimura,[3,4] and Yuya Sakuraba[2,†]

[1]*Materials Sciences Research Center, Japan Atomic Energy Agency, Hyogo 679-5148, Japan*
[2]*Research Center for Magnetic and Spintronic Materials, National Institute for Materials Science, Sengen 1-2-1, Tsukuba 305-0047, Japan*
[3]*Graduate School of Advanced Science and Engineering, Hiroshima University, 1-3-1 Kagamiyama, Higashi-Hiroshima 739-8526, Japan*
[4]*International Institute for Sustainability with Knotted Chiral Meta Matter (SKCM^2), 1-3-1 Kagamiyama, Higashi-Hiroshima 739-8526, Japan*

(Received 29 July 2023; revised 15 October 2023; accepted 6 November 2023; published 1 December 2023)

We investigated the element-specific electronic structure of a half-metallic Weyl ferromagnet candidate Co_2FeSi film by utilizing soft-x-ray resonant photoelectron spectroscopy and first-principles calculations with and without considering an on-site Coulomb interaction. An Fe $2p-3d$ resonant photoelectron experiment revealed that the Fe $3d$ states exist around 2 and 4 eV below the Fermi energy. Our calculations, based on the generalized gradient approximation without considering a Coulomb interaction at the Fe site, successfully reproduced the experimentally observed Fe $3d$ partial density of states. Our findings shed light on the highly controversial correlation effect of Co_2FeSi, offering valuable insights into its half metallicity and Weyl semimetallicity.

DOI: 10.1103/PhysRevB.108.L241101

Half-metallic ferromagnets are considered key materials for spintronic applications due to their perfect spin polarization (P) at the Fermi energy (E_F) resulting from peculiar electronic structures, where the density of states (DOS) for one spin channel is finite at E_F, while the DOS for the opposite spin channel exhibits a semiconducting gap. First-principles calculations predict many half-metallic ferromagnet candidates in oxides, sulfides, and Heusler alloys [1–6]. Among them, Co-based Heusler alloys, such as Co_2MnSi, Co_2MnGe, and Co_2FeSi, exhibit very high Curie temperatures (e.g., ∼1100 K in Co_2FeSi [7]) compared to the other candidates. Over the past two decades, the performance of tunnel magnetoresistance (TMR) and giant magnetoresistance devices using Co-based Heusler alloys as ferromagnetic electrodes has improved dramatically [8–14]. Indeed, a TMR ratio exceeding 1900% has been achieved in epitaxial $Co_2MnSi/MgO/Co_2MnSi$ magnetic tunnel junctions at low temperature [15].

For ferromagnetic Heusler alloys, it is empirically known that the Slater-Pauling rule ($M = N_v - 24$) exists, where M is the magnetic moment, and N_v is the valence electron number [16]. According to this rule, Co_2MnSi and Co_2MnGe ($N_v = 29$) are expected to be $M = 5\mu_B$, while Co_2FeSi ($N_v = 30$) is expected to have $6\mu_B$. Macroscopic magnetometry measurements on Co_2FeSi have confirmed $M = 5.97\mu_B$ at 5 K in bulk samples [7]. However, the calculated M using the local density approximation (LDA) approach yields a considerably smaller value ($\sim 5\mu_B$) [17]. To address this discrepancy, on-site Coulomb interactions (U) are often customarily incorporated into the calculations [18–23]. By considering certain U in the range of 2.5–5.0 eV for Co and 2.5–4.5 eV for Fe, Co_2FeSi exhibits a half-metallic electronic structure with $M = 6\mu_B$, whereas it becomes an ordinary ferromagnet without assuming U [17].

Electrical transport and magnetotransport measurements have revealed a half-metallic-like behavior in Co_2FeSi at low temperatures. Specifically, a nonlinear quadratic curve of the temperature-dependent resistivity and the positive ordinary magnetoresistance effect indicate the suppression of electron-magnon scattering due to the half-metallic nature, but only at low temperature [24]. Additionally, a negative anisotropic magnetoresistance (AMR) ratio, which has been reported as a required feature of half-metallic material, is observed at 10 K [25]. However, the sign of the AMR ratio turns positive around 300 K, whereas other half-metallic candidates, such as Co_2MnSi and $Co_2FeGa_{0.5}Ge_{0.5}$, show almost temperature-independent behaviors [26]. These results suggest that the minority-spin conduction band edge of Co_2FeSi is close to E_F, and the half-metallic behavior collapses around 300 K due to the thermal excitation.

Moreover, it has been theoretically proposed that several Co-based Heusler alloys, such as Co_2MnGa and Co_2MnAl, are classified as ferromagnetic Weyl semimetals [27], and recently, their topologically nontrivial band dispersions have been experimentally verified by angle-resolved photoelectron spectroscopy [28–30]. These alloys have multiple Weyl cones or nodal lines near E_F and exhibit giant anomalous Hall and Nernst effects due to a large Berry curvature in momentum

*Present address: Hiroshima Synchrotron Radiation Center, Hiroshima University, 2-313 Kagamiyama, Higashi-Hiroshima 739-0046, Japan; sumidak1126@hiroshima-u.ac.jp
†SAKURABA.Yuya@nims.go.jp

 ©2023 American Physical Society

space [28,29,31–33]. Co_2FeSi is also predicted to possess Weyl cones with their nodes slightly above E_F, suggesting the possibility of large anomalous transverse transport properties emerging by electron doping [34,35]. However, since both the half metallicity and the anomalous transverse transport property are significantly influenced by on-site Coulomb interactions, it is crucially important to experimentally investigate the role of the correlation effect in Co_2FeSi.

In this Letter, we have investigated the element-specific electronic structure of the half-metallic Weyl ferromagnet candidate, Co_2FeSi film, using resonant photoelectron spectroscopy (RPES) and first-principles calculations with and without considering the on-site Coulomb interactions. By conducting RPES measurements in a Fe $2p-3d$ core absorption region, we have successfully extracted the Fe $3d$ partial DOS from the valence band. Our findings tell us that Fe $3d$ states exist around 2 and 4 eV below E_F. More importantly, the observed peak positions of Fe $3d$ states are well reproduced by calculations without assuming Coulomb interactions at the Fe site.

An epitaxial thin-film of (001)-oriented Co_2FeSi was deposited on a MgO(001) substrate by the magnetron sputtering method. First, the MgO(001) substrate was annealed at 600 °C for 30 min, followed by the deposition of buffer layers of Cr (20 nm) and Ag (80 nm) at room temperature (RT). Then, the Cr/Ag buffer layers were annealed at 300 °C for 30 min to smooth the sample surface. A 20-nm-thick Co_2FeSi layer was deposited on the Cr/Ag buffer at RT and annealed at 550 °C for 30 min to obtain the $L2_1$-ordered structure. To prevent surface oxidization, a 1-nm-thick Al-capping layer was deposited on the sample at RT. Using a conventional x-ray diffractometer, we clearly observed a 002 superlattice peak from $B2$ ordering and a 111 superlattice peak from $L2_1$ ordering of the Co_2FeSi film in $\theta-2\theta$ x-ray diffraction (XRD) profiles by setting the scattering vector to the out-of-plane and the ⟨111⟩ direction, respectively (see Supplemental Material Fig. S1 [36]). These results suggest the epitaxial growth of the Co_2FeSi film. From the observed XRD peaks, we evaluated the degrees of $B2$ and $L2_1$ ordering, which are expressed as $S_{B2}=\sqrt{\frac{I^{obs}_{002}/I^{obs}_{004}}{I^{sim}_{002}/I^{sim}_{004}}}$ and $S_{L2_1}=\sqrt{\frac{I^{obs}_{111}/I^{obs}_{444}}{I^{sim}_{111}/I^{sim}_{444}}}$, respectively, where I^{obs}_{hkl} (I^{sim}_{hkl}) is the observed (simulated) hkl peak intensity. I^{sim}_{hkl} was calculated by VESTA [37]. The S_{B2} and S_{L2_1} values of the Co_2FeSi layer were estimated to be ∼1.10 and ∼0.74, respectively. The S_{B2} value is close to 1, suggesting the existence of nearly perfect $B2$ ordering. Although the $L2_1$ ordering is still not perfect, the estimated large S_{L2_1} value indicates the existence of the highly ordered $L2_1$ phase. The actual chemical composition of the fabricated film was confirmed to be $Co_{1.93}Fe_{1.16}Si_{0.91}$ by x-ray fluorescence spectrometry.

RPES and x-ray absorption spectroscopy (XAS) experiments were performed at the twin-helical undulator beamline BL23SU equipped with a hemispherical electron analyzer (VG Scienta SES-2002) at SPring-8 [38]. The circularly polarized soft x-ray beam was used for the measurements. The energy resolution was set to 140 meV at 700 eV. The XAS spectra were acquired in the total electron yield mode. During the experiments, the temperature was kept at 30 K.

First-principles calculations for the $L2_1$-ordered Co_2FeSi were conducted within the density-functional theory using the full-potential linearized augmented plane-wave method as implemented in the WIEN2K code [39] with use of the generalized gradient approximation (GGA) [40] and GGA+U approaches. The experimentally verified lattice constant (5.635 Å) was used for the calculations. The Brillouin zone integration was conducted using a uniform 21 × 21 × 21 mesh. The plane-wave cutoff parameter RK_{max} was set at 9.0. We calculated P given by

$$P=\frac{D_\uparrow(E_F)-D_\downarrow(E_F)}{D_\uparrow(E_F)+D_\downarrow(E_F)},$$

where $D_\uparrow(E_F)$ [$D_\downarrow(E_F)$] indicates the DOS at E_F for the majority-spin (minority-spin) channel.

Figure 1(a) displays the calculated total DOS as well as Co $3d$ and Fe $3d$ partial DOS for Co_2FeSi without considering the on-site Coulomb interaction ($U=0$ eV). Here, the majority- and minority-spin states are separately shown in the upper and lower parts. The Co $3d$ and Fe $3d$ states mainly contribute to the total DOS, while the contributions of the s and p states are negligibly small (see Supplemental Material Figs. S2 and S3 [36]). In the minority-spin channel, a gap structure is seen just below E_F. However, since the Fe $3d$ partial DOS crosses E_F [see the inset of Fig. 1(a)], the calculated P is −0.57,

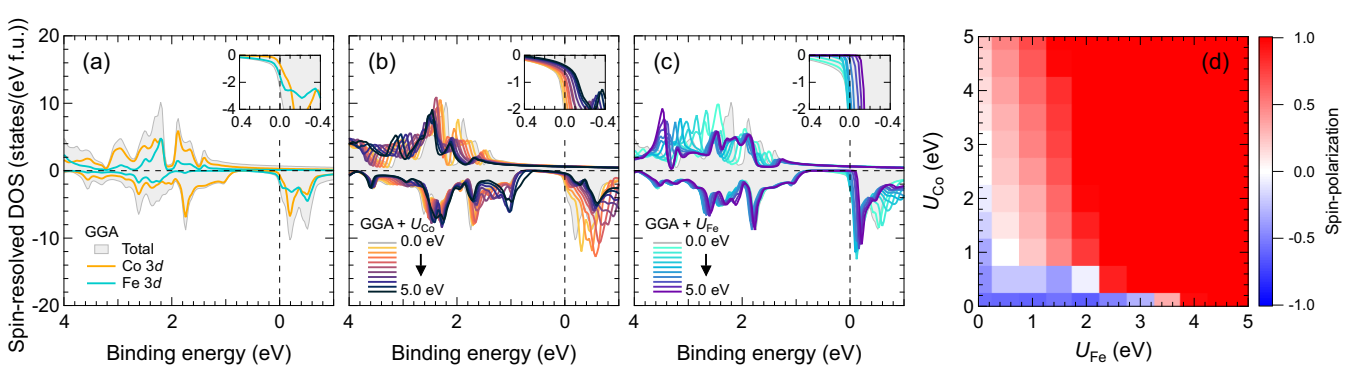

FIG. 1. Calculated DOS and spin polarization. (a) Calculated total and partial DOS for Co_2FeSi without considering the on-site Coulomb interactions ($U_{Co}=U_{Fe}=0.0$ eV). The inset shows the magnified DOS near E_F in the minority-spin channel. (b) Calculated total DOS with U_{Co} ranging from 0.0 to 5.0 eV in 0.5 eV steps, while U_{Fe} is fixed at 0.0 eV. (c) Same as (b), but with U_{Fe} ranging from 0.0 to 5.0 eV in 0.5 eV steps, while U_{Co} is fixed at 0.0 eV. (d) Spin-polarization map in $U_{Co}-U_{Fe}$ parameter space.

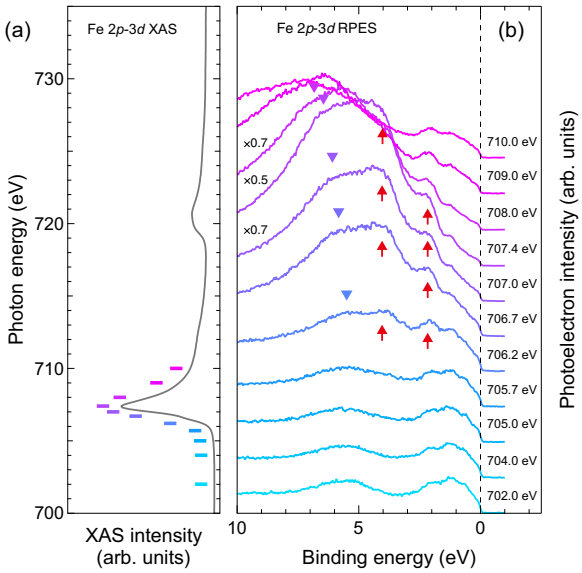

FIG. 2. XAS and valence band PES spectra in the Fe $2p-3d$ core absorption region. (a) XAS spectrum at the Fe $L_{2,3}$ $(2p-3d)$ edge. (b) Valence band PES spectra in the Fe $2p-3d$ core absorption region. Colored lines in (a) denote the excitation energies for PES measurements. Red arrows and inverted triangles in (b) indicate the resonant photoelectron and normal Auger components, respectively.

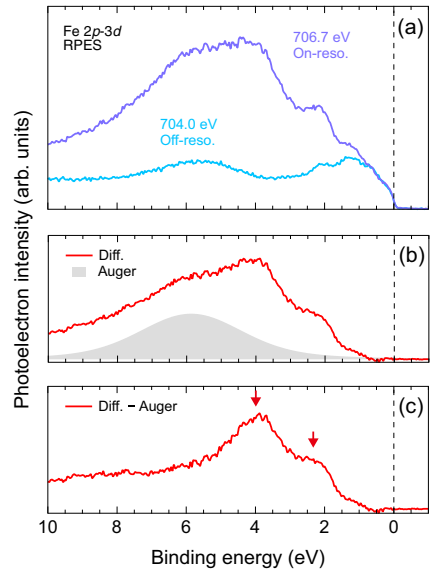

FIG. 3. RPES spectra and decomposition analysis of the Auger component. (a) On-resonant and off-resonant PES spectra taken at 706.7 and 704.0 eV, respectively. (b) Difference spectrum obtained by subtracting the off-resonant spectrum from the on-resonant spectrum. The gray shaded area represents the Auger component fitted by using a Voigt function. (c) Fe $3d$ partial DOS spectrum obtained by subtracting the Auger component from the difference spectrum.

indicating that Co_2FeSi does not exhibit half metallicity at $U = 0$ eV.

Figure 1(b) shows the calculated total DOS with various on-site Coulomb interactions for $3d$ orbitals at the Co site (U_{Co}), while that at the Fe site (U_{Fe}) is set to 0.0 eV. We confirmed that the bottom of the conduction band in the minority-spin channel crosses E_F even at $U_{Co} = 5.0$ eV [see the inset of Fig. 1(b)], although the conduction band peak, located around -0.2 eV, is systematically shifted away from E_F with increasing U_{Co}. On the other hand, when the U_{Fe} is introduced instead of the U_{Co}, the minority-spin DOS at E_F is substantially decreased with increasing U_{Fe} [Fig. 1(c)]. At $U_{Fe} \geqslant 4.0$ eV, P becomes 1.0 (half metallic) [see the inset of Fig. 1(c)]. Figure 1(d) summarizes the calculated P in the $U_{Co} - U_{Fe}$ parameter space. Here, red and blue colors represent positive and negative P values. Since the minority-spin edge is mainly composed of the Fe $3d$ state, the half-metallic electronic structure cannot be realized without U_{Fe}.

To experimentally verify the role of U_{Fe}, we performed RPES in the Fe $2p-3d$ core absorption region. Figure 2(a) shows the XAS spectrum at the Fe $L_{2,3}$ $(2p-3d)$ edge. The observed XAS spectrum exhibits clear peaks at the Fe L_3 and L_2 edges, which are consistent with the previously reported results [7,20,41], and no additional structure due to oxidation has been found. The excitation energies for the RPES measurements are depicted by the colored lines in Fig. 2(a). Figure 2(b) shows the valence band spectra in the Fe $2p-3d$ core absorption region ($h\nu = 702$–710 eV). These spectra were normalized by the photoelectron intensities of the shallow Si $2p$ core level, which does not contribute to the resonant process. In the energy range from 702.0 to 705.7 eV (prior to $2p-3d$ core absorption), no marked change in the spectral shape is found. On the other hand, we observed a significant enhancement in photoelectron intensities above $h\nu = 706.2$ eV, indicating the occurrence of Fe $2p-3d$ resonance. Notably, three enhanced peaks located at 2.0, 4.0, and 5.5 eV were found, for instance, at 706.2 eV. The former two peaks, marked by red arrows, remain at the same binding energy independent of $h\nu$. This enhancement can be classified as the resonant photoelectron process and described by Fe $2p^6 3d^n \rightarrow 2p^5 3d^{n+1} \rightarrow 2p^6 3d^{n-1} + e^-$. On the other hand, the location of the latter peaks, marked by inverted triangles, systematically shifts toward a higher binding energy with increasing $h\nu$. Thus, it can be classified as a normal Auger component, described by Fe $2p^6 3d^n \rightarrow 2p^5 3d^{n+1} \rightarrow 2p^6 3d^{n-2} + e^-$. Note that RPES was also conducted in the Co $2p-3d$ core absorption region (see Supplemental Material Fig. S5 [36]). However, due to the dominant normal Auger signals, possibly caused by the prohibited resonant process between the unoccupied Co $3d$ e_u state and the occupied Co $3d$ e_g state [42], the resonant feature was hardly seen.

In order to extract the Fe $3d$ partial DOS from the RPES spectra, we compare the resonant spectrum observed at 706.7 eV, where the normal Auger contribution is relatively small, with the nonresonant spectrum observed at 704.0 eV [Fig. 3(a)]. It is evident that the photoelectron intensity increases below 1 eV at 706.7 eV due to both the Fe $2p-3d$ resonant and normal Auger processes, while there appears to be little change around E_F. To highlight the difference, Fig. 3(b) shows the difference spectrum obtained by subtracting the nonresonant spectrum from the resonant one shown in Fig. 3(a). Here, we fitted the normal Auger component with a Voigt function, as depicted by the gray shaded area. Figure 3(c) represents the spectrum after subtracting the

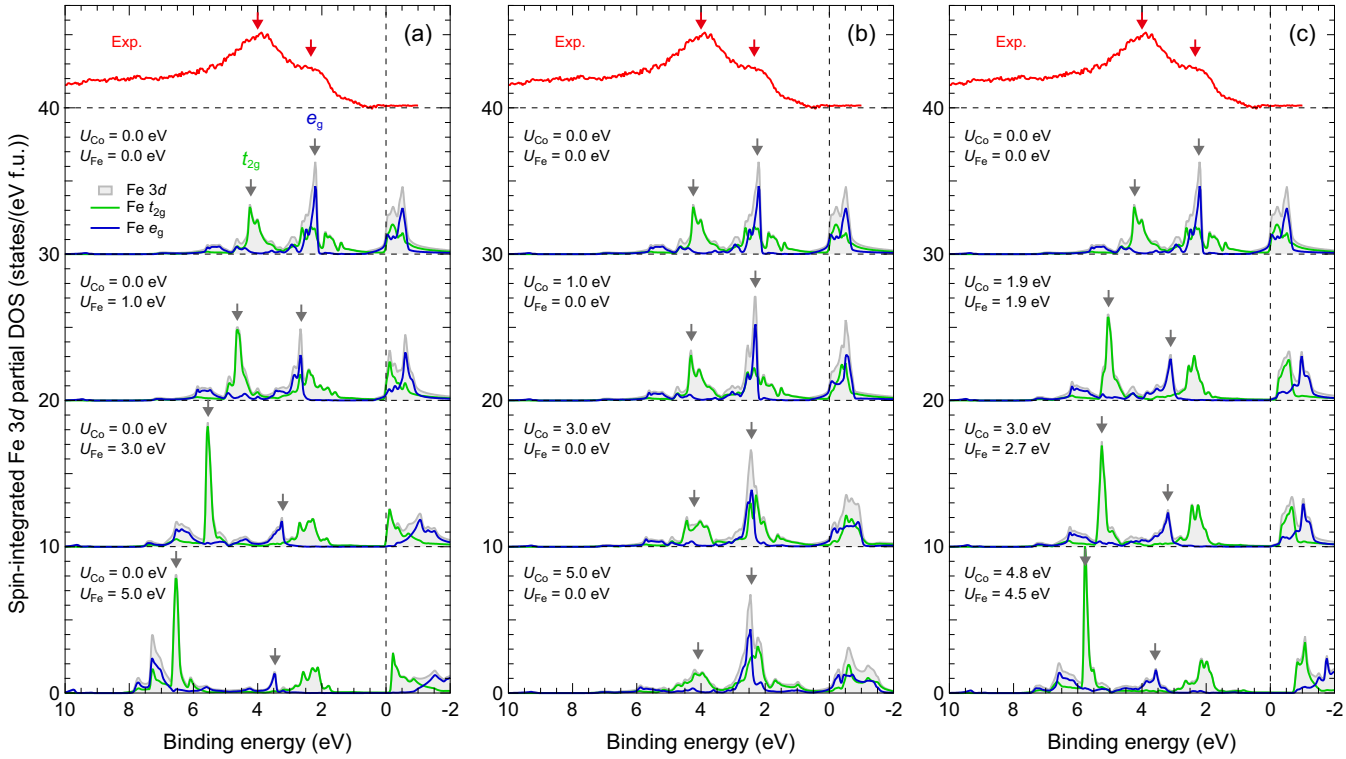

FIG. 4. Fe 3*d* partial DOS with various U_{Co} and U_{Fe} values. (a) Comparison of experimentally obtained Fe 3*d* partial DOS with calculations with $U_{Fe} = 0.0$, 1.0, 3.0, and 5.0 eV, while U_{Co} is fixed at 0.0 eV. (b) Same as (a), but with $U_{Co} = 0.0$, 1.0, 3.0, and 5.0 eV, while U_{Fe} is fixed at 0.0 eV. (c) Same as (a) and (b), but with $U_{Co} = 1.9$ eV, $U_{Fe} = 1.9$ eV within GGA+*U* [20], $U_{Co} = 3.0$ eV, $U_{Fe} = 2.7$ eV within GGA + *U* [19], and $U_{Co} = 4.8$ eV, $U_{Fe} = 4.5$ eV within LDA+*U* [7]. Blue and green lines correspond to the Fe e_g and t_{2g} states, respectively.

Auger component from the difference spectrum, which reflects the Fe 3*d* partial DOS. This result signifies the presence of prominent Fe 3*d* partial DOS peaks around 2 and 4 eV.

We discuss the role of on-site Coulomb interactions by comparing the experimentally obtained Fe 3*d* partial DOS with theoretical calculations using various values of U_{Co} and U_{Fe}. Figure 4(a) displays the theoretically calculated Fe 3*d* partial DOS (lower curves) with $U_{Fe} = 0.0$, 1.0, 3.0, and 5.0 eV, while U_{Co} is set to 0.0 eV, alongside the experimentally obtained DOS (upper curve). For the case of $U_{Fe} = 0.0$ eV, we find a sharp peak mainly composed of the e_g state at 2.2 eV and another peak composed of the t_{2g} state at 4.2 eV. In addition, a shoulder structure around 1.5 eV is seen. These distinct features are consistent with the experimental result. When U_{Fe} is increased to 1.0 eV, the shape of partial DOS remains almost the same as that for $U_{Fe} = 0.0$ eV, but the peaks are slightly shifted to 2.7 and 4.6 eV. As U_{Fe} is further increased, both the e_g and t_{2g} peaks systematically shift toward a higher binding energy, and the partial DOS at E_F is decreased, i.e., a half metallicity sets in at $U_{Fe} = 5.0$ eV. Among these, the theoretically obtained result for $U_{Fe} = 0.0$ eV is closest to the experimental one, suggesting that the Coulomb interaction at the Fe site is very small. In Fig. 4(b), we also calculated the Fe 3*d* partial DOS with $U_{Co} = 0.0$, 1.0, 3.0, and 5.0 eV, whereas U_{Fe} is fixed to 0.0 eV. In sharp contrast to the results shown in Fig. 4(a), U_{Co} has little effect on the Fe 3*d* partial DOS. Specifically, the peak positions of the occupied state remain almost unchanged when U_{Co} is varied, and the Fe 3*d* states cross E_F (not half metallic). In Fig. 4(c), we further compare the Fe 3*d* partial DOS using the previously reported values within the GGA+*U* and LDA+*U* approaches with the experimental results. Nonetheless, the calculations with U_{Fe} fail to reproduce the experimentally captured features. Considering all the findings, we conclude that the U_{Fe} value in Co_2FeSi is negligibly small, suggesting that Co_2FeSi does not have a perfectly spin-polarized state at E_F.

Note that the calculated *P* for $U_{Fe} = 0$ eV and $U_{Co} = 0$–5 eV, ranging from −0.57 to 0.25, is inconsistent with the high *P* values expected by the transport measurements at low temperatures [24–26]. To address this discrepancy, we have calculated the spin polarization derived from the *s*, *p* orbitals (P_{sp}) (see Supplemental Material Fig. S2 [36]). This is because the conductivity is dominated by the *s*, *p* orbitals due to their relatively small effective masses compared to the localized *d* orbitals [43]. The calculated P_{sp} for $U_{Fe} = 0$ eV and $U_{Co} = 0$–5 eV shows high positive values ranging from 0.42 to 0.94, which are consistent with the transport measurements. Moreover, the *P* values determined by the point-contact Andreev reflection measurements (0.4–0.6) are also included in this range [44–47].

Now we comment on the role of U_{Co}. As seen in Fig. 4(b), the presence of U_{Co} has a minor impact on the electronic structure of the occupied states, but it leads to significant changes in the unoccupied electronic structure (see also Supplemental Material Fig. S4 [36]). As a result, the presence or absence of U_{Co} may influence the anomalous transverse transport properties and the topological nature of the system. We hope that the

role of U_{Co} will be further elucidated through future investigations employing other element-specific techniques, such as resonant inelastic x-ray scattering.

In conclusion, we investigated the electronic structure of the potential half-metallic Weyl ferromagnet candidate Co_2FeSi film using element-specific RPES in the Fe $2p-3d$ core excitation region and first-principles calculations based on the GGA+U approach. We experimentally found that the Fe $3d$ states exist around 2 and 4 eV below E_F. These features are well reproduced by the calculation without considering U_{Fe}. While the role of U_{Co} remains subject to further discussion, it appears likely that Co_2FeSi does not exhibit a half-metallic electronic structure.

The RPES and XAS measurements were performed at SPring-8 BL23SU (Proposals No. 2021A3811 and No. 2022A3811). This work was financially supported by KAKENHI (Grants No. 17H06152, No. 21K14540, and No. 21H01608), JST CREST (Grant No. JPMJCR21O1), and JST ERATO "Magnetic Thermal Management Materials" (Grant No. JPMJER2201). We thank Yukiharu Takeda and Goro Shibata for valuable discussions.

[1] R. A. de Groot, F. M. Mueller, P. G. van Engen, and K. H. J. Buschow, Phys. Rev. Lett. **50**, 2024 (1983).
[2] J. Kübler, A. R. Williams, and C. B. Sommers, Phys. Rev. B **28**, 1745 (1983).
[3] K. Schwarz, J. Phys. F: Met. Phys. **16**, L211 (1986).
[4] W. E. Pickett and D. J. Singh, J. Magn. Magn. Mater. **172**, 237 (1997).
[5] S. K. Kwon, S. J. Youn, and B. I. Min, Phys. Rev. B **62**, 357 (2000).
[6] S. Picozzi, A. Continenza, and A. J. Freeman, Phys. Rev. B **66**, 094421 (2002).
[7] S. Wurmehl, G. H. Fecher, H. C. Kandpal, V. Ksenofontov, C. Felser, H.-J. Lin, and J. Morais, Phys. Rev. B **72**, 184434 (2005).
[8] S. Kämmerer, A. Thomas, A. Hütten, and G. Reiss, Appl. Phys. Lett. **85**, 79 (2004).
[9] Y. Sakuraba, M. Hattori, M. Oogane, Y. Ando, H. Kato, A. Sakuma, T. Miyazaki, and H. Kubota, Appl. Phys. Lett. **88**, 192508 (2006).
[10] T. M. Nakatani, T. Furubayashi, S. Kasai, H. Sukegawa, Y. K. Takahashi, S. Mitani, and K. Hono, Appl. Phys. Lett. **96**, 212501 (2010).
[11] M. J. Carey, S. Maat, S. Chandrashekariaih, J. A. Katine, W. Chen, B. York, and J. R. Childress, J. Appl. Phys. **109**, 093912 (2011).
[12] J. Sato, M. Oogane, H. Naganuma, and Y. Ando, Appl. Phys. Express **4**, 113005 (2011).
[13] Y. Sakuraba, M. Ueda, Y. Miura, K. Sato, S. Bosu, K. Saito, M. Shirai, T. J. Konno, and K. Takanashi, Appl. Phys. Lett. **101**, 252408 (2012).
[14] K. Elphick, W. Frost, M. Samiepour, T. Kubota, K. Takanashi, H. Sukegawa, S. Mitani, and A. Hirohata, Sci. Technol. Adv. Mater. **22**, 235 (2021).
[15] H.-X. Liu, Y. Honda, T. Taira, K.-i. Matsuda, M. Arita, T. Uemura, and M. Yamamoto, Appl. Phys. Lett. **101**, 132418 (2012).
[16] I. Galanakis, P. H. Dederichs, and N. Papanikolaou, Phys. Rev. B **66**, 174429 (2002).
[17] H. C. Kandpal, G. H. Fecher, C. Felser, and G. Schonhense, Phys. Rev. B **73**, 094422 (2006).
[18] H. C. Herper, B. Krumme, D. Ebke, C. Antoniak, C. Weis, A. Warland, A. Hütten, H. Wende, and P. Entel, J. Appl. Phys. **109**, 07E128 (2011).
[19] M. Kallmayer, P. Klaer, H. Schneider, G. Jakob, H. J. Elmers, D. Legut, and P. M. Oppeneer, Phys. Rev. B **84**, 054448 (2011).
[20] M. Meinert, J.-M. Schmalhorst, M. Glas, G. Reiss, E. Arenholz, T. Bohnert, and K. Nielsch, Phys. Rev. B **86**, 054420 (2012).
[21] M. Veis, L. Beran, R. Antos, D. Legut, J. Hamrle, J. Pistora, Ch. Sterwerf, M. Meinert, J.-M. Schmalhorst, T. Kuschel, and G. Reiss, J. Appl. Phys. **115**, 17A927 (2014).
[22] B. Abderrahim, M. Ameri, D. Bensaid, Y. Azaz, B. Doumi, Y. Al-Douri, and F. Benzoudji, J. Supercond. Novel Magn. **29**, 277 (2016).
[23] K. Nawa and Y. Miura, RSC Adv. **9**, 30462 (2019).
[24] D. Bombor, C. G. F. Blum, O. Volkonskiy, S. Rodan, S. Wurmehl, C. Hess, and B. Buchner, Phys. Rev. Lett. **110**, 066601 (2013).
[25] Y. Sakuraba, S. Kokado, Y. Hirayama, T. Furubayashi, H. Sukegawa, S. Li, Y. K. Takahashi, and K. Hono, Appl. Phys. Lett. **104**, 172407 (2014).
[26] V. K. Kushwaha, S. Kokado, S. Kasai, Y. Miura, T. Nakatani, R. Kumara, H. Tajiri, T. Furubayashi, K. Hono, and Y. Sakuraba, Phys. Rev. Mater. **6**, 064411 (2022).
[27] J. Kübler and C. Felser, Europhys. Lett. **114**, 47005 (2016).
[28] I. Belopolski, K. Manna, D. S. Sanchez, G. Chang, B. Ernst, J. Yin, S. S. Zhang, T. Cochran, N. Shumiya, H. Zheng, B. Singh, G. Bian, D. Multer, M. Litskevich, X. Zhou, S.-M. Huang, B. Wang, T.-R. Chang, S.-Y. Xu, A. Bansil *et al.*, Science **365**, 1278 (2019).
[29] K. Sumida, Y. Sakuraba, K. Masuda, T. Kono, M. Kakoki, K. Goto, W. Zhou, K. Miyamoto, Y. Miura, T. Okuda, and A. Kimura, Commun. Mater. **1**, 89 (2020).
[30] T. Kono, M. Kakoki, T. Yoshikawa, X. Wang, K. Sumida, T. Muro, K. Goto, Y. Sakuraba, R. Y. Umetsu, and A. Kimura, Phys. Rev. B **104**, 195112 (2021).
[31] A. Sakai, Y. P. Mizuta, A. A. Nugroho, R. Sihombing, T. Koretsune, M.-T. Suzuki, N. Takemori, R. Ishii, D. Nishio-Hamane, R. Arita, P. Goswami, and S. Nakatsuji, Nat. Phys. **14**, 1119 (2018).
[32] S. N. Guin, K. Manna, J. Noky, S. J. Watzman, C. Fu, N. Kumar, W. Schnelle, C. Shekhar, Y. Sun, J. Gooth, and C. Felser, NPG Asia Mater. **11**, 16 (2019).
[33] P. Li, J. Koo, W. Ning, J. Li, L. Miao, L. Min, Y. Zhu, Y. Wang, N. Alem, C.-X. Liu, Z. Mao, and B. Yan, Nat. Commun. **11**, 3476 (2020).
[34] H.-L. Huang, J.-C. Tung, and G.-Y. Guo, Phys. Rev. B **91**, 134409 (2015).
[35] J. Noky, Y. Zhang, J. Gooth, C. Felser, and Y. Sun, npj Comput. Mater. **6**, 77 (2020).
[36] See Supplemental Material at http://link.aps.org/supplemental/10.1103/PhysRevB.108.L241101 for x-ray diffraction profiles,

calculated partial DOS, spin polarization, band structure, and RPES spectra in the Co $2p-3d$ core absorption region.

[37] K. Momma and F. Izumi, J. Appl. Crystallogr. **44**, 1272 (2011).

[38] Y. Saitoh, Y. Fukuda, Y. Takeda, H. Yamagami, S. Takahashi, Y. Asano, T. Hara, K. Shirasawa, M. Takeuchi, T. Tanaka, and H. Kitamura, J. Synchrotron Radiat. **19**, 388 (2012).

[39] P. Blaha, K. Schwarz, F. Tran, R. Laskowski, G. K. H. Madsen, and L. D. Marks, J. Chem. Phys. **152**, 074101 (2020).

[40] J. P. Perdew, K. Burke, and M. Ernzerhof, Phys. Rev. Lett. **77**, 3865 (1996).

[41] S. Wurmehl, G. H. Fecher, H. C. Kandpal, V. Ksenofontov, C. Felser, and H.-J. Lin, Appl. Phys. Lett. **88**, 032503 (2006).

[42] T. Kono, M. Kakoki, T. Yoshikawa, X. Wang, K. Sumida, K. Miyamoto, T. Muro, Y. Takeda, Y. Saitoh, K. Goto, Y. Sakuraba, K. Hono, and A. Kimura, Phys. Rev. B **100**, 165120 (2019).

[43] Y. Kota, T. Takahashi, H. Tsuchiura, and A. Sakuma, J. Appl. Phys. **105**, 07B716 (2009).

[44] Z. Gercsi, A. Rajanikanth, Y. K. Takahashi, K. Hono, M. Kikuchi, N. Tezuka, and K. Inomata, Appl. Phys. Lett. **89**, 082512 (2006).

[45] T. M. Nakatani, A. Rajanikanth, Z. Gercsi, Y. K. Takahashi, K. Inomata, and K. Hono, J. Appl. Phys. **102**, 033916 (2007).

[46] S. V. Karthik, A. Rajanikanth, T. M. Nakatani, Z. Gercsi, Y. K. Takahashi, T. Furubayashi, K. Inomata, and K. Hono, J. Appl. Phys. **102**, 043903 (2007).

[47] L. Makinistian, M. M. Faiz, R. P. Panguluri, B. Balke, S. Wurmehl, C. Felser, E. A. Albanesi, A. G. Petukhov, and B. Nadgorny, Phys. Rev. B **87**, 220402(R) (2013).